Growth and structure of gold films on a Re($10\bar{1}0$) surface

2009 J. Phys.: Condens. Matter 21 134012

(http://iopscience.iop.org/0953-8984/21/13/134012)

J. Phys.: Condens. Matter **21** (2009) 134012 (12pp) doi:10.1088/0953-8984/21/13/134012

Growth and structure of gold films on a Re(10$\bar{1}$0) surface

C Pauls and K Christmann

Institut für Chemie und Biochemie der FU Berlin, Bereich Physikalische und Theoretische Chemie, Takustrasse 3, D-14195 Berlin, Germany

Received 2 October 2008
Published 12 March 2009
Online at stacks.iop.org/JPhysCM/21/134012

Abstract

We have deposited Au films in ultra-high vacuum onto a rhenium (10$\bar{1}$0) surface in submonolayer and multilayer concentrations and studied them by means of low- and medium-energy electron diffraction in the temperature range between 300 and 800 K. In the submonolayer range, Au forms several low-energy electron diffraction (LEED) phases, namely, a (1 × 3), a (1 × 4), a (1 × 5) and a (1 × 6) phase, consisting of one-dimensionally ordered Au chains in the [1$\bar{2}$10] direction, until the formation of a complete pseudomorphic monolayer is indicated by a (1 × 1) LEED phase. In the multilayer regime, a (1 × 8) LEED phase appears over a surprisingly wide coverage range from about two to at least eight monolayers, which we interpret as a hexagonal uniaxially compressed reconstructed Au overlayer on pseudomorphically grown hexagonal close-packed gold layers. In order to get access to absolute Au coverages, we have performed LEED (I, V) measurements and carried out a LEED structure determination for the (1 × 1) phase. We propose the formation of a full Au monolayer in which both the Re trough and top-row sites are being covered by Au atoms. The data are discussed and compared with those from previous studies on related systems.

1. Introduction

The growth of thin metal films on refractory metal surfaces has been studied since the early days of surface science, and chemists and physicists have focused on the kinetics and thermodynamics of growth, especially the growth mechanism, as well as on the structure and physical properties of the deposited films. Depending on the relative size of the substrate/deposit atoms and their electronic configuration, the film growth may either proceed pseudomorphically, whereby the structural parameters of the overlayer material are forced to adapt to the substrate, or the deposit grows with its own characteristic lattice parameters in this hetero-epitactic process. For both growth modes, there exist numerous examples in the literature, which obey the general growth principles, but in addition often display a wealth of subtle details characteristic of the individual systems. For more information, the reader is referred to fundamental articles and reviews by Bauer [1–3]; in addition, there exist several review articles in the field of metal-on-metal deposition, because these systems are believed to play an essential role as model systems for bimetallic catalysis [4–6]. Historically, the data published in the literature can be subdivided to studies lasting perhaps up to the mid-1960s, whereby mostly electron microscopy and x-ray diffraction techniques were used to obtain structural information. There followed a period ranging from about 1964 to about 1986, in which the respective properties were deduced mainly from low-energy electron diffraction (LEED) and related techniques. The latest information on both growth mechanisms and structural properties of thin metal film, since the invention and development of scanning tunneling microscopy [7], was at least supported by scanning-probe microscopy techniques. However, due to problems of contrast and image formation in SPM, really *accurate* surface structure determinations can hardly be gained, and this is why careful LEED studies supplemented by full-dynamical LEED calculations are unrenounceable even today, when reliable structure information is aspired. We just mention that the Tensor LEED program packages developed in the groups of van Hove and Heinz at the Universities of California and Erlangen, respectively, are particularly helpful here [8–10]. Besides the determination of the locations of the deposited atoms or molecules, their binding energy to the substrate as well as their mutual interactions (which are responsible for submonolayer phases with long-range order) are of major scientific interest. This latter information is mostly obtained from combined LEED, XPS and thermal desorption spectroscopy studies [11–14].

Here, we report on the observation of a sequence of ordered phases formed by gold atoms that are deposited onto a corrugated Re substrate and on a LEED structure determination of a pseudomorphic (1 × 1) Au overlayer using among others the aforementioned Tensor LEED method of the Erlangen group.

2. Experimental and computational details

2.1. The experimental set-up

The experiments were carried out in a standard stainless steel ultra-high vacuum (UHV) chamber that was equipped with the standard facilities to clean and characterize a metal single-crystal surface, i.e., Auger electron spectroscopy using a four-grid LEED optics as high-pass filter in conjunction with an external electron gun, a quadrupole mass spectrometer (Balzers Prisma) for residual gas monitoring, an Ar ion sputter gun for surface cleaning (Leybold, IQ 35), and a 4-grid reverse-view LEED optics (Omikron) for LEED measurements, see below. Further experimental details can be found elsewhere [15]. In addition, a home-made device for performing medium-energy electron diffraction (MEED) was attached to the chamber. It consisted of an electron gun spanning the energy range from ∼1000 to 5000 eV (VSW EG5) and was mounted in a way to allow grazing incidence of the electron beam on the sample (incidence angle ∼88° with respect to the surface normal) and a transparent phosphorous screen on a counter flange where the intensity of the directly reflected (0, 0) electron beam could be monitored and measured by a TV camera set-up.

The ultrapure Re(10$\bar{1}$0) sample (5N, MaTeck) was x-ray oriented to the (10$\bar{1}$0) direction, cut and polished to within 0.2°, and mounted on the manipulator between two parallel-running 0.5 mm Re wires. High-temperature access was obtained by means of either resistive heating (T_{max} = 1600 K) or by electron bombardment (T_{max} = 2300 K), whereby the temperature was controlled with a Re/WRe thermocouple; the resistive heating was performed using a programmable power supply (TET electronics) and appropriate computer software. The chamber was evacuated by a combined turbo-molecular and titanium sublimation pumping system. High-purity research-grade gases (carbon monoxide, oxygen, argon) were taken from 'Minican' gas cylinders and admitted to the UHV system via a bakeable leak valves. The pressure in the chamber was measured by an ion gauge of the Bayard–Alpert type (Varian); after appropriate baking and pumping the base pressure in the chamber was in the low 10^{-10} mbar range. We emphasize here that even traces of active residual gases, especially carbon monoxide CO, can considerably influence and alter the formation of the ordered gold phases as will be communicated in a forthcoming article [16].

As described in detail elsewhere [15–17], sample cleaning was achieved by several cycles of gentle O_2/H_2 oxidation/reduction cycles and subsequent high-temperature flashing and annealing; the surface cleanliness was repeatedly controlled by AES and LEED.

The Au deposition was performed using a commercial electron beam evaporator (Omikron EFM4); the deposition rates could be varied within wide limits, typically, evaporation rates around a few monolayers per hour were chosen with the surface temperature held at 800 K. This ensured a homogeneous, thermodynamically-controlled growth and the appropriate formation of Au phases with well-developed Au chain ordering. From previous measurements by Wagner [14, 18], who studied the Au desorption from the Re(0001) surface, one can estimate that thermal Au desorption is still insignificant at 800 K; the Au desorption rate is less than 10^{-8} ML s^{-1}.

Concerning the Au coverage calibration, we use the common definition that the coverage Θ = 1.0 corresponds to the situation in which as many Au atoms are present in the surface as there exist Re atoms in the topmost layer, i.e. are located in the ridges of the surface. In the unreconstructed (10$\bar{1}$0) surface, the atomic density is N_{Re} = 8.142 × 10^{18} atoms m^{-2}. Hence, we understand the (hypothetical) Au coverage Θ = 1 as if only every Re row atom carries one adsorbed Au atom (at the moment irrespective of any deviations between the atomic diameters)—the Re trough atoms still remain uncovered in this counting.

2.2. Computational procedure

The LEED (I, V) curves were always collected at room temperature using a computer-controlled video technique [19]. By very careful mounting and sample adjustment we achieved an accurate normal electron beam incidence with incidence angles δ between the surface normal and the electron beam of less than 0.5 (±0.2) degrees. Due to a μ-metal shielded vacuum chamber the residual magnetic stray fields were low enough to rule out a variation of the incidence angle with electron energy. The normal electron beam incidence was repeatedly checked by measuring the I, V curves of the four symmetry-equivalent first-order diffraction beams of the clean Re surface. Generally, the measured LEED images were stored and subsequently analyzed using the photometry software IRAF [20]. Spurious scattered light contributions were subtracted by fitting a Gauß distribution to the background pixel values around the respective diffraction spots. As usual, all beam intensity data were normalized with respect to the primary electron beam current.

The LEED intensity analysis was performed in two steps. In the beginning, a couple of plausible structure models (= Au adsorption sites) were selected. Then the theoretical I, V curves were coarsely calculated using the symmetrized automated tensor LEED I, V program package of van Hove *et al* [8, 9]. The results of this first 'grid search' were critically analyzed with respect to the Pendry R factor [21], and in a second step only those structures were admitted to a more refined LEED calculation that yielded an R factor below 0.40. More details will be described in section 3.2.

3. Results and discussion

3.1. Overview

As mentioned above, Au atoms deposited onto a clean Re(10$\bar{1}$0) surface form, as function of surface concentration,

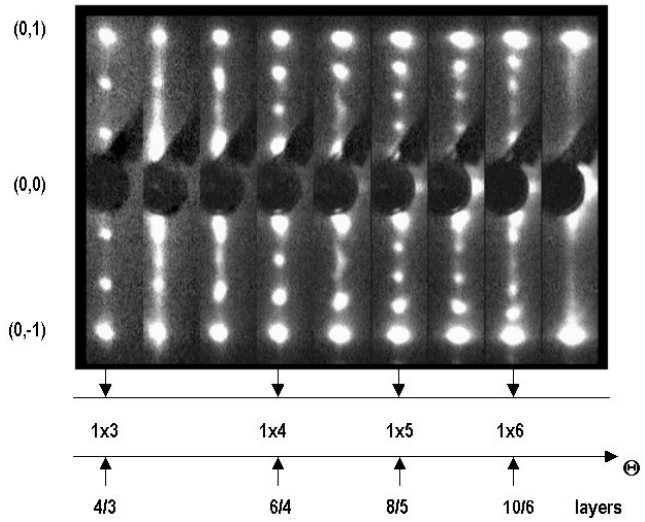

Figure 1. Series of Au-induced LEED patterns in the submonolayer coverage regime at $E = 26$ eV showing the development of the $(1 \times n)$ phases with $n = 3, 4, 5$ and 6. Indicated are also the coverages in Au monolayers. See the text for further details.

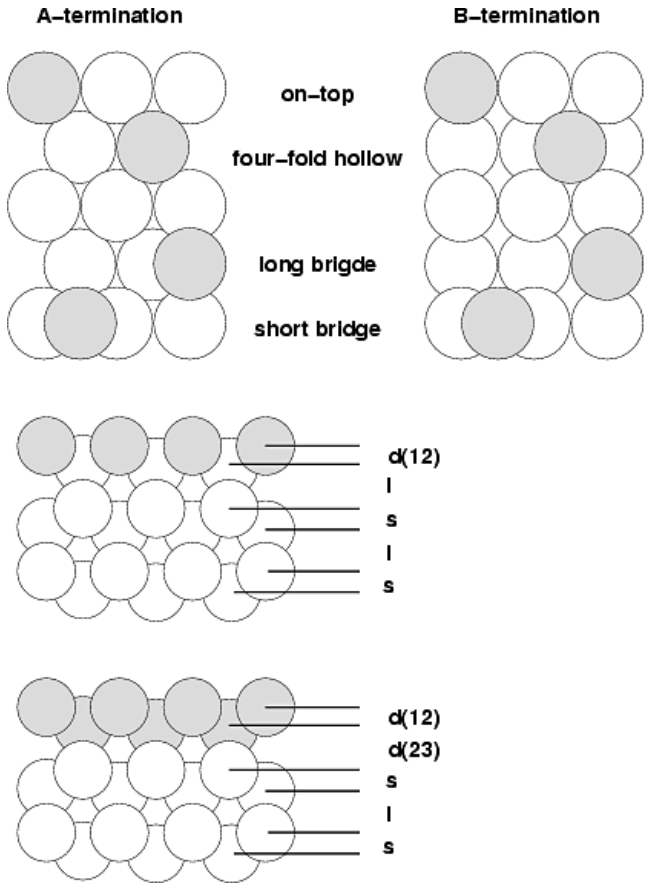

Figure 2. Surface crystallography of the hcp(10$\bar{1}$0) surface with possible adsorption sites for hetero-atoms (such as Au) indicated by shading. Top left: 'A' termination; top right: 'B' termination (see the text for further details). Considered are the relevant top, 4-fold hollow and long- and short-bridge sites. To illustrate possible double layer formation, also perpendicular cuts through the Re surface are shown including the stacking sequence of the topmost six layers, whereby the possible cases of a single and a double monolayer (bilayer) are distinguished by shading. Note the different layer distances (l = large, s = small) within the Re (Au) topmost layers.

various submonolayer phases resulting in $(1 \times n)$ LEED patterns, followed by a phase that produces a clear (1×1) LEED pattern, and a multilayer phase showing a (1×8) LEED structure over a surprisingly large range of deposited layers (at least 8 ML). The submonolayer phenomena are summarized in figure 1 as a sequence of Au coverage-dependent LEED images. For convenience, only the reciprocal space between the $(0, 1)$ and $(0, -1)$ beams is shown taken from screen shots at an electron energy of 26 eV, where the Au-induced fractional-order LEED spots appear most clearly. In the bottom of the figure a tentative Au coverage scale is drawn based on our coverage calibration for the complete Au monolayer (ML, see below) which confirmed that the 'full' ML of the (1×1) phase actually represents a gold bilayer ($\Theta = 2, 0$).

The presentation and discussion of our data will be organized as follows: first, we give a short introduction to the termination problem of the clean Re(10$\bar{1}$0) surface before we expand on the preparation and structure determination of the (1×1) Au phase using MEED and LEED, because it simply represents a continuation of the stacking of the Re layers in the (10$\bar{1}$0)-oriented crystal. As this (1×1) phase has been subjected to a quantitative LEED calculation, we expand in this section also on how the calculations have been carried out. In the second subchapter, we will describe the formation of the *submonolayer* Au phases, and finally, in the third sub-section, we are going to present the data on the (1×8) *multilayer* phase.

3.2. The clean Re surface and the Au monolayer (1 × 1) phase

After appropriate cleaning and annealing, the clean Re(10$\bar{1}$0) surface showed a LEED pattern with extremely sharp and bright diffraction spots on a very low background. When working with hcp metal surfaces, we recall that the (10$\bar{1}$0) orientation can exist in two different terminations 'A' and 'B' which differ with respect to their spacings between adjacent atomic layers (causing a different surface corrugation) as well as with regard to the registry of the first and second layer. Previous LEED structure analyses of the clean Re(10$\bar{1}$0) surface always established the less corrugated 'A' termination and indicated in addition a pronounced multilayer relaxation. While Davis and Zehner [22] reported on a large first-to-second layer contraction of 17%, later work by Döll *et al* [23]—although mainly concerned with a structural analysis of hydrogen atomic layers adsorbed on the Re(10$\bar{1}$0) surface—confirmed likewise the 'A' termination but revealed a considerably smaller inward relaxation of merely 5% (which may have, however, been affected by spurious H adsorption). Since in the context of Au deposition and layer growth the knowledge of the correct surface termination is essential we have performed another LEED analysis (not presented here) which again revealed the 'A' termination and resulted in a somewhat larger first-to-second layer contraction of 12.2% [24]. For the sake of convenience, we recall once again the crystallography of the hcp (10$\bar{1}$0) surface in figure 2 and indicate in addition the possible adsorption sites for

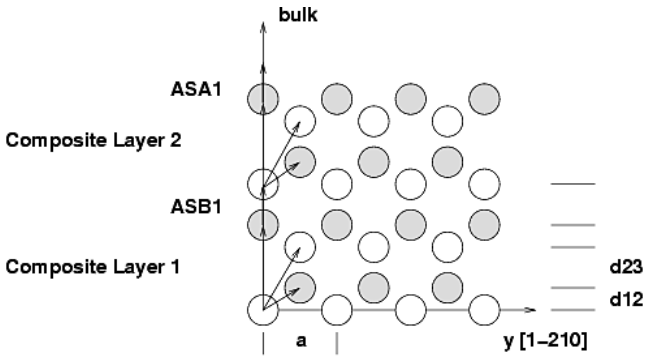

Figure 3. Illustration of the stacking sequence of atomic layers perpendicular to the surface (from bottom to top) and the combination of adjacent layers to so-called 'composite layers' used in the LEED program packages. The notations ASA1 and ASB1 stand for the vectors describing the interlayer spacings between the composite layers. Shown as arrows are also the vectors connecting the scatterers within the individual composite layers.

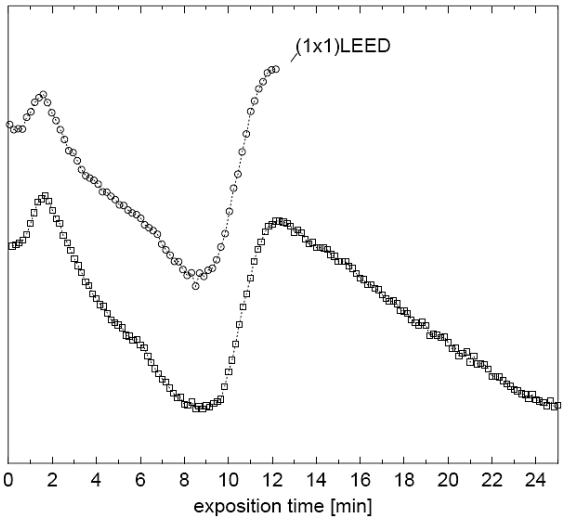

Figure 4. Two MEED curves (intensity of the directly reflected 5 keV electron beam *versus* the Au deposition time t_{evap} (minutes)). The two curves were successively obtained under the same experimental conditions, the individual measuring points are indicated by squares and circles, respectively. The curves exhibit two pronounced intensity maxima separated by a deep minimum. See the text for details.

hetero-atoms (such as Au) by shaded circles. We confine ourselves to the full monolayer situation and consider only the practically relevant top, 4-fold hollow and long- and short-bridge sites, respectively; i.e., sites that have the same symmetry as the substrate surface. Note that *both hcp terminations, A and B, can provide the respective sites* which leads already to eight different sub-structures for the Au monolayer. If we include the possibility that *all exposed* Re surface atoms (in the ridges and troughs) can actually carry a deposit atom we must admit also the formation of a *double layer* on top—leading altogether to 16 sub-structures. To illustrate this double layer formation, we present in figure 2 also perpendicular cuts through the surface of the Re crystal showing the stacking sequence of the topmost layers, and indicate both a single monolayer and a double layer (bilayer) by shading. Furthermore, we mark the perpendicular layer distances (l = large, s = small) within the Re (Au) topmost layers. Because of the short layer distances perpendicular to the $(10\bar{1}0)$ orientation it is essential for obtaining a sufficient convergence in the LEED calculations to build up the crystal by comprising adjacent layers with short mutual distance, leading to a minimum of 2 layer-stacks ('composite layers') as indicated in figure 3. In our calculation, actually 4-layer stacks were chosen.

It is deemed useful at this point to expand somewhat on another method that we used in our study. Besides LEED, medium-energy electron diffraction (MEED) turned out to be a very helpful *in situ* monitor of the kind and progress of the Au deposition and the associated coverages at T = 800 K. In this respect, MEED has been widely used in the past, for example to follow the growth of Co films on a Cu substrate [25]. In figure 4, two typical MEED curves are displayed, with the intensity of the directly reflected (0, 0) beam plotted *versus* the deposition time t_{evap}, the electron beam energy being 5 keV. The two curves were successively obtained under the same experimental conditions and prove the degree of reproducibility as far as the film properties, but also as far as the constancy of the evaporation source is concerned. This ensures that we could use t_{evap} as a convenient coverage monitor. The fine structure of the MEED curves shows two pronounced intensity maxima separated by a deep minimum around $t_{evap} \approx 9$ min as well as some (rather insignificant) wiggles between 4 and 7 min. The first maximum appears shortly after the deposition started, namely, at about $t_{evap} \approx 2$ min, the other one after $t_{evap} \approx 12$ min. The occurrence of the second maximum always coincides with the fully developed pseudomorphic (1 × 1) LEED pattern and is a clear indication for a smooth surface that acts as a 'mirror' for the grazing incidence MEED electrons. At very small coverages and sufficiently high temperatures (as in our deposition experiment), the Au atoms form a homogeneous 2D lattice gas, where the Au atoms are believed to decorate and heal the inherent step and defect sites of the clean Re surface. This should lead to an improved smoothening, since we know from thermal desorption data on other Re surfaces that the defect densities are about 3–5% of the monolayer density [11–14]. However, as soon as the coverage increases, 2D solid Au islands become stable in equilibrium with the still existing lattice gas and lead to an increased roughness of the surface. This in turn causes a progressive decrease of the MEED intensity until a minimum is reached at Au coverages where the whole surface is covered by (1 × 3) islands. If the Au deposition is continued after the first MEED minimum, we find a steep re-increase until a sharp second maximum is formed which coincides, as mentioned above, exactly with the Au coverage necessary to form the complete Au bilayer, cf, section 3.2. Apparently, this (1 × 1) layer has a similar 'electron reflectivity' as the Au-decorated Re$(10\bar{1}0)$ surface.

Returning to the surface structure determination, we have performed coarse LEED calculations in which a reduced experimental data set of only four diffracted beams (0, 1; 1,

Table 1. *R* factors obtained for the different (1 × 1) test structures.

Structure #	Site	Termination of Re surface	# of Au layers	Pendry *R* factor
1	Long bridge	A	1	0.558
2	4-fold	A	1	0.741
3	Atop	A	1	0.812
4	Short bridge	A	1	0.732
5	Long bridge	B	1	0.733
6	4-fold	B	1	0.383
7	Short bridge	B	1	0.680
8	Atop	B	2	0.812
9	Long bridge	B	2	0.588
10	4-fold	B	2	0.898
11	Atop	B	2	0.817
12	Short bridge	B	2	0.795
13	Long bridge	A	2	0.751
14	4-fold	A	2	0.262
15	Short bridge	A	2	0.692
16	Atop	A	2	0.818

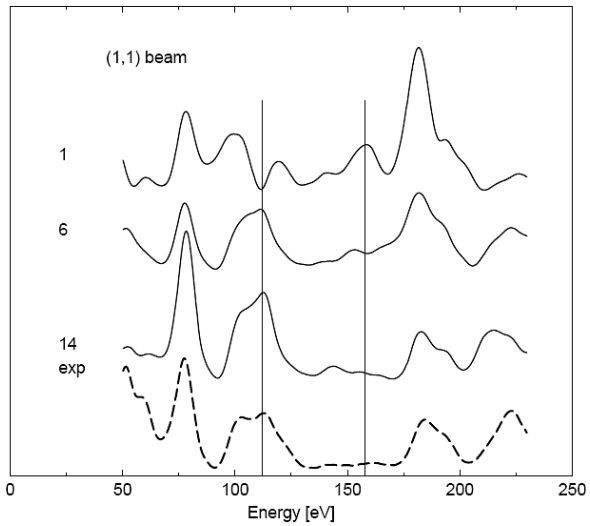

Figure 5. Theoretical *I*, *V* curves calculated for the (1, 1) beam within a first coarse grid search, in comparison with the experiment (dashed bottom curve). The top curve belongs to a structure that does not fit (#1 with *R* factor $R_P = 0.558$, Au atoms in the long-bridge site of termination 'A'), the middle curve (#6) assumes Au atoms only in the top layer of a Re surface with termination 'B' leading to $R_P = 0.38$. The second curve from bottom refers to structure #14 (the first and the second monolayer consist of Au atoms on the 'A'-terminated Re surface) and shows even at a first glance the best agreement with the experiment which is reflected also in the *R* factor of $R_P = 0.26$ (as a guide for the eye we have drawn vertical lines to demonstrate the coincidence of the maxima). Accordingly, the two structures #6 and #14 have been selected for a refined LEED calculation.

0; 1, 1; and 2, 0) in an energy interval from 50 to 230 eV was used with an overall energy width of merely 720 eV. The intensity analysis as well as the (relativistic) computation of the scattering phases was carried out using the Barbieri/van Hove symmetrized automated Tensor LEED package [8, 9] coupled with an *R* factor-directed automated search algorithm. In these calculations, only the inner potential and the two outermost layer distances were varied; thermal vibrations were considered by assuming fixed Debye temperatures of 170 K for Au and 415 K for Re. Because of the limited energy range the expansion of the scattering potential could be limited to only 9 coefficients leading to short computation times and a rather fast grid search. Table 1 gives an overview of the 16 tested structure models and the *R* factors obtained. From all the structures tested only two yield a reasonable *R* factor < 0.4, namely the structure #14 (bilayer Au on the 'A' termination, four-fold coordinated sites) with $R = 0.26$, and structure #6 (monolayer Au on the 'B' termination, four-fold coordinated site) with $R = 0.383$. To illustrate the kind of agreement we present, in figure 5, three calculated *I*, *V* curves for the (1, 1) beam with the experiment, one of them belonging to a structure that does definitely not fit (#1 with $R = 0.558$), where the Au atoms are assumed in the long-bridge site of the monolayer on top of termination 'A' (top *I*, *V* curve), and the two *I*, *V* curves that gave the best *R* factors (structures #6 and 14). At the first glance, one can understand why these two latter structures are significantly better than the rest of the choices. In both models the geometric array of the scatterers is practically identical; both of them lead to a pseudomorphic growth (except some minor relaxations). The Au atoms are thereby located in positions of the Re surface that simply lead to a continuation of the lattice. The only (but apparently decisive) difference between structures #6 and #14 is that in structure #14 the first and the second monolayer consists of Au atoms while in structure #6 the second layer is made up of Re atoms of termination 'B'. While it is, in principle, possible to distinguish in the LEED *I*, *V*-behavior between chemically different scatterers [26–28], difficulties arise because of the quite similar electron densities of Au (nuclear charge +79 units) and Re (+75 units). This is why we subjected *both* structures with the best *R* factor to a refined LEED analysis, although structure #6 is physically less likely than structure #14, because a reconstruction of an 'A'-terminated Re surface to a 'B'-terminated is thermodynamically certainly less favorable.

In the refined LEED analysis then the layer distances between the third and fourth and the fourth and fifth layers were additionally varied as well as the respective vibrational amplitudes. Furthermore, the data base was extended to all available *I*, *V* data which led to a width of 2177 eV as documented in table 2 and helped to improve the significance of the data considerably. Because of the better flexibility concerning the choice of the parameters to be varied the calculations were carried out using the TensErLEED programs developed at the University of Erlangen [29, 30]. Since the atomic phase shifts appear to depend slightly on the chemical environment, we calculated new phase shifts for the Au atoms of the two topmost layers and for the Re atoms of the topmost Re layer, respectively. The extended energy range ΔE required an expansion of the phase shifts up to angular momenta of $L = 12$ (for safety, we used $L_{max} = 14$), whereby the (relativistic) computation was again carried out using the program of the van Hove library. It is known that often a substantial improvement between experimental and theoretical data can be achieved by making the inner crystal-potential energy-dependent [29]. For this purpose we first selected energy intervals 50 eV wide and

Table 2. Recorded beams of the (1 × 1) Au phase and their energy ranges.

Order of diffraction (beam #)	Minimum energy E_{min} (eV)	Maximum energy E_{max} (eV)	Energy width ΔE (eV)
(0, 1)	35	347	313
(1, 0)	40	347	308
(1, 1)	58	290	233
(0, 2)	58	330	273
(1, 2)	102	347	246
(0, 3)	142	347	206
(2, 0)	142	347	206
(2, 1)	142	347	206
(1, 3)	162	347	186
Sum (ΔE)			2177

optimized the values for the respective inner potential. These data are shown in figure 6 together with a fit function $V_R(E)$ (solid line):

$$V_R(E) = V_0 + \frac{\alpha}{\sqrt{E - E_0}}$$

with the fit parameters $\alpha = -28.2$, $V_0 = -8.75$ eV and $E_0 = -24.26$ eV. In the final calculation the function $V(E)$ was indeed used and led to a slight improvement of the Pendry R factor, $\Delta R_P = -0.02$. On the other hand, the thus obtained data did not deviate significantly from those calculated by means of an energy-independent inner potential; the maximum change in bond lengths was 0.01 Å. In order to avoid errors due to the use of the Tensor LEED approximation the thus obtained optimum geometry was then carefully checked by a full-dynamical LEED calculation. The R_P factor is calculated as an average over the individual R_P factors of the respective LEED beams, whereby their contribution is weighed by the measured energy width given in table 2. Due to the higher-dimensional parameter space the R factor went considerably lower for both structure models (#6 and #14). For the pseudomorphic bilayer (#14) we obtained $R_P = 0.17$, whilst structure #6 (single Au layer on top of Re termination 'B') yielded $R_P = 0.24$. The respective LEED I, V curves for the pseudomorphic bilayer are shown in figure 7. The statistical error range of both Pendry R factors can be determined using the energy width of the data (ΔE), the imaginary part of the inner potential, V_i, (=5 eV) and the respective Pendry R factor [26, 31] according to

$$\mathrm{var}(R_P) = R_P \sqrt{\frac{8V_i}{\Delta E}}.$$

The obtained error interval of 0.023 for $R_P = 0.17$ clearly excludes the next-best structure (#6) with $R_P = 0.24$ and thus confirms the pseudomorphic bilayer as the true surface configuration. We add that the two upper layer distances ($d_{12} = 0.82$ Å and $d_{23} = 1.69$ Å) are slightly expanded (3% and 6%, respectively) compared with the ideal Re hcp lattice while the deeper layers do not deviate anymore from the Re bulk lattice parameters. The Debye temperatures of the Au layers are determined to be 165 K (first layer) and 230 K (second layer).

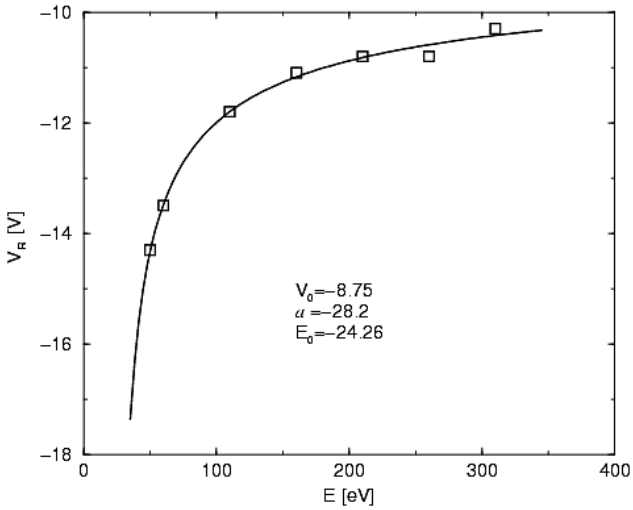

Figure 6. Optimization of the energy-dependent inner potential $V_R(E)$. $V_R(E)$ was calculated within selected energy intervals of 50 eV according to a fit function (solid line, see text) with the fit parameters $\alpha = -28.2$, $V_0 = -8.75$ eV and $E_0 = -24.26$ eV. In this way the R factor could be improved by $\Delta R_P = -0.02$.

3.3. Ordered Au phases in the submonolayer coverage range

Next we turn to Au coverages $\Theta < 2$ (= submonolayer concentrations in our coverage definition) which lead to the formation of various (1 × n) Au phases with long-range order as shown in figure 1. In order to achieve the optimum LEED superstructures, the Re crystal temperature had to be kept close to 800 K during deposition; lower temperatures, especially $T < 600$ K, reduce the long-range order and produce merely streaky LEED patterns (with streaks in (0, ±k) direction).

During the very first stages of the Au deposition, a slightly increasing diffuse LEED background without any 'extra' spots indicates the formation of a disordered Au lattice gas phase.

The first well-ordered overlayer phase is definitely a (1×3) phase; the intensity maximum of the fractional-order LEED spots is reached after a deposition time t_{evap} of about 3.3 min. If this is related to t_{evap} associated with the full bilayer ($\Theta = 2$) we end up with a coverage of $\Theta_{1\times3} = 4/3 = 1.33$. It is remarkable that the (1 × 3) structure appears for the first time already at a coverage of ∼0.28 and persists up to $\Theta = 1.33$, when a gradual shift and splitting of the 'extra' spots begins. Furthermore, we note an almost linear increase in intensity of the fractional-order beams up to the nominal coverage $\Theta_{1\times3}$. The respective situation is depicted in figure 8 which shows the intensity of the (0, 1/3) and (0, 2/3) LEED spots (electron energy 26 eV) as a function of the Au coverage Θ at a temperature of 400 K. Also shown for comparison is the (practically coverage-independent) intensity of an integer-order (0, 1) LEED spot in the top of the figure. The linear increase of the fractional-order beam intensity is indicative of island-like growth of large (1 × 3) domains (large compared to the LEED transfer width) [32, 33]. The overall situation in the coverage range $0.3 < \Theta < 1.33$ can then be described by an equilibrium in which (1 × 3) Au islands coexist with a homogeneous Au lattice gas phase. The Au adsorbate consists of spatially separated homogeneous phases

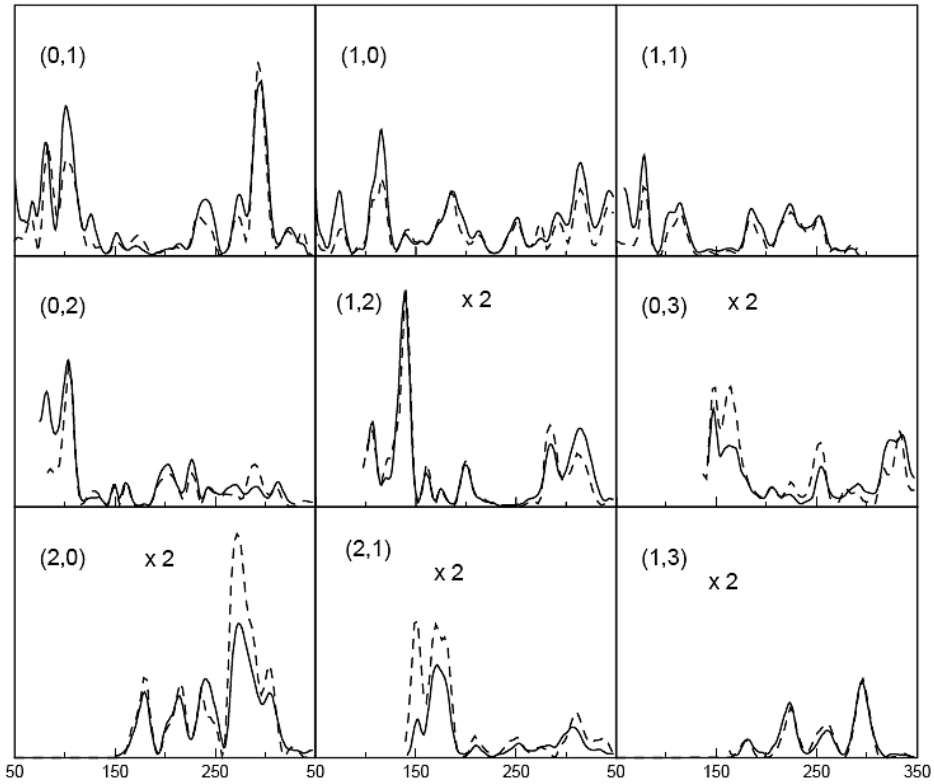

Figure 7. Compilation of experimental (dotted lines) and theoretical LEED I, V curves (full lines) that have been calculated for structure #14 by means of a full-dynamical calculation. Shown are nine different beams in the energy range from 50 to 250 eV. In all cases, there is good agreement between experiment and theory.

with different densities, and as the coverage increases at a given temperature, the equilibrium is shifted in favor of the higher-density phase. We further note that the lower limit of the (1×3) phase, i.e., $\Theta = 0.28$, coincides exactly with the first intensity maximum observed in the MEED experiment, cf figure 4, thus supporting the idea that the beginning appearance of '2D solid' (1×3) islands impair the reflectivity for MEED electrons in the grazing incidence mode.

The (1×3) pattern suggests a three-fold periodicity in [0001] direction as compared to the Re substrate lattice. This is illustrated in the (tentative) structure model of figure 9(a) which contains Au triple chains parallel to the $[1\bar{2}10]$ direction interrupted in [0001] direction by single Au chains pointing to attractive Au–Au interactions in $[1\bar{2}10]$ direction. It is noteworthy that the Au atoms apparently match the Re lattice in this direction, because they exhibit the same lattice vector. This means that the effective diameter of the Au atoms ($d_{\mathrm{Au}} = 2.884$ Å) has to shrink by almost 4%. Similar effects are known from other, related hetero-epitactic systems, for example, Au on Ru$(10\bar{1}0)$ [34]. A hint to the still empty Re sites left and right from the single-atom Au chain is provided by titration experiments with carbon monoxide. CO thermal desorption spectra clearly prove that CO can still adsorb in the respective Re sites, however, with a strongly reduced adsorption energy of merely 45–50 kJ mol^{-1} as compared to 95–120 kJ mol^{-1} found for molecular CO desorption from bare Re$(10\bar{1}0)$ [15]. This strong reduction is certainly caused by the proximity of the Au atoms [16, 24], since, e.g., on the Au(110) surface CO adsorbs in a γ state with $E_{\mathrm{des}} = 38.5$ kJ mol^{-1} [35], and on

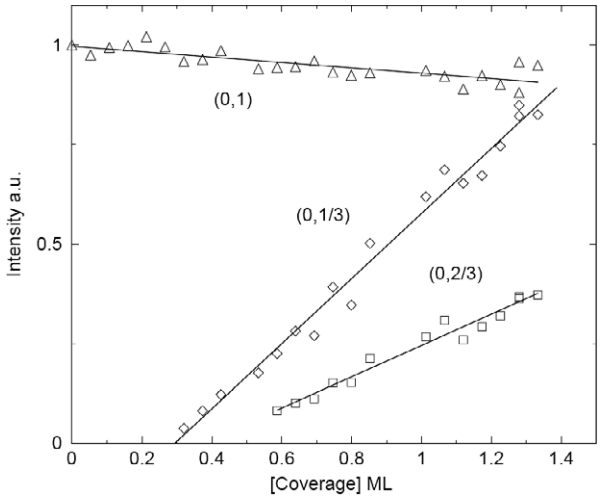

Figure 8. Plot of the intensity of the (0, 1/3) and (0, 2/3) LEED spots of the (1×3) Au phase (electron energy 26 eV) as a function of the Au coverage Θ at a temperature of 400 K. The 'extra' intensity increases almost linearly with Au coverage pointing to island-like growth of large (1×3) domains. Also shown for comparison is the (practically coverage-independent) intensity of an integer-order (0, 1) LEED spot in the top of the figure.

the completely with Au covered Re$(10\bar{1}0)$ surface ($\Theta = 2$) we find likewise this γ state, whilst for $1 < \Theta_{\mathrm{Au}} < 2$ a narrow split state γ_1 and γ_2 appears reflecting CO that adsorbs on the Au patches of the surface and CO that is still in contact with Re

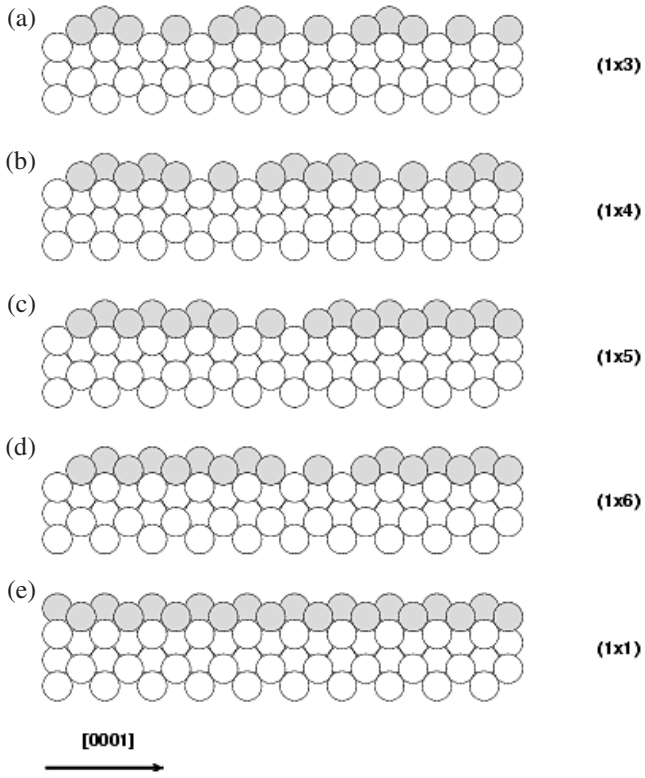

Figure 9. Ball models representing perpendicular cuts through the Re surface (open circles) covered with the $(1 \times n)$ Au structures (shaded circles). Starting from Au triple chains in the top (1×3) phase over quintuple Au chains in the (1×4) and septuple chains in the (1×5) structure finally the closed (1×1) phase is obtained which actually consists of an Au double layer: No Re surface atoms are accessible anymore.

surface atoms. Latest on the (1×1) Au overlayer the splitting disappears, and the remaining single γ CO desorption state clearly demonstrates the *bilayer* character of this overlayer.

Upon increasing the Au coverage beyond $\Theta = 4/3$ the fractional-order LEED spots become elongated in [0001] direction and slightly shift their positions until they reach the quarter positions and form a well-developed (1×4) structure after $t_{\text{evap}} \approx 5$ min, cf, figure 1. This is a clear indication that the growth mechanism resembles the one described many years ago by Ertl and Rau for oxygen adsorption on a Pd(110) surface, where a continuous splitting and shift of the fractional-order diffraction spots were explained by a coherent superposition of (1×2) and (1×3) oxygen domains [36]. In our case, (1×4) domains gradually grow at the expense of (1×3) domains. According to the structure model of the (1×3) phase we just extend the respective model by introducing now five-fold Au chains that are interrupted by single Au chains, cf, figure 9(b). The overall Au coverage then is $\Theta_{1\times4} = 1.5$. There follows again a small coverage region with streaky and split spots, until a LEED pattern of a clear (1×5) structure can be seen, completely analogue to the (1×6) structure that appears upon further deposition. The explanation is as before, and we present the respective structure models in figures 9(c) (1×5) and (d) (1×6) with the associated coverages of $\Theta_{1\times5} = 8/5 = 1.6$ and $\Theta_{1\times6} = 5/3 = 1.67$. Note that the respective LEED patterns are not easy to obtain, careful annealing and relatively low deposition rates are required to achieve the best ordering. Hypothetically, (1×7) and (1×8) phases with coverages of $12/7 = 1.71$ and $14/8 = 1.75$, respectively, are expected next, however, we did not attempt to resolve these structures because our (relatively coarse) Au coverage increments ($\Delta\Theta \approx 0.055$) did not allow us to follow the respective development of ordering in the elevated Au coverage regime. Instead we only observed somewhat structured, i.e. k-dependent diffraction intensity between the (0, 0) and $(0, \pm1)$ spots as evident from figure 1. A general formula relating the periodicity n with the coverage $\Theta_{1\times n}$ is

$$\Theta_{1\times n}(n) = \frac{2(n-1)}{n}.$$

Quite clearly though the 'extra' intensity between the (0, 0) and $(0, \pm1)$ beams *disappeared completely* at slightly higher Au coverages giving rise to a background free and sharp (1×1) LEED pattern. We note that the respective vanishing of fractional-order beam intensity occurs only in a sharp and well-defined coverage interval and entirely coincides with the second MEED maximum that we observed after $t_{\text{evap}} = 12$ min, cf, figure 4. As discussed in detail in section 3.2 and proven by a quantitative LEED intensity analysis, this (1×1) phase represents a pseudomorphic gold bilayer with the coverage $\Theta_{1\times1} = 2.0$ and can be taken as a basis for a later Stranski–Krastanov or Frank–van-der-Merwe type of growth. cf section 3.4.

At this point it is useful to compare our data with a similar investigation of Au deposition on the ruthenium $(10\bar{1}0)$ surface reported some years ago by Poulston *et al* [34] who employed combined LEED, TDS, Auger electron and x-ray photoelectron spectroscopy. The Ru$(10\bar{1}0)$ surface has the same structure as the respective Re surface, the only difference being the slightly smaller (∼3%) atomic diameter of Ru ($d_{\text{Ru}} = 2.695$ Å, $d_{\text{Re}} = 2,775$ Å). Interestingly, the authors reported likewise on the appearance of Au $(1 \times n)$ submonolayer structures ($n = 3, 4, 5, \ldots$), but did not observe a (1×1) LEED pattern and, hence, definitely *excluded the existence of a pseudomorphic Au layer* at a coverage of $\Theta = 2$. Otherwise and in agreement with our definition they associated the ordered Au phases with adsorbed *bilayer* chains and arrived at coverages $\Theta_{1\times3} = 1.33$, $\Theta_{1\times4} = 1.5$ etc. The Au chain formation was explained by attractive Au–Au interactions which followed also from an analysis of their thermal desorption spectra [34], since the (coverage-dependent) desorption energy revealed a marked increase of E_{des} with Θ_{Au}, namely, 85 kJ mol^{-1}. Although we did not explicitly measure thermal desorption spectra for the Au + Re$(10\bar{1}0)$ system, we have TD data for the Au + Re(0001) system at our disposal [14, 18] which clearly show strong attractive Au–Au interactions with an increase of E_{des} from ∼280 kJ mol^{-1} at very small coverages to ∼380 kJ mol^{-1} for the complete monolayer. Likewise in agreement with our observation is the surprisingly extended coverage range in which the authors observed the (1×3) LEED pattern. They explained this finding by assuming significant attractive interactions between the Au atoms leading—as in our

case—to a comparatively large-coverage region in which 2D Au islands and Au lattice gas coexist. Their most remarkable observation, however, is—as already stated above—the lack of an (1 × 1) Au phase on Ru(10$\bar{1}$0) which led the authors to exclude a pseudomorphic growth of Au—in contrast to the basal Ru(0001) plane, where just this growth had been repeatedly reported [37, 38], and, of course, in contrast to our present result with the Au/Re(10$\bar{1}$0) system, where just this pseudomorphic (1 × 1) layer is a key feature. We will return to this point in section 3.4 when we present and discuss the Au multilayer growth. Here, we add a thermodynamic argument in favor of a complete 'wetting' of the Re surface by Au atoms, namely, the relatively similar surface free energies of the two metals, cf, $\gamma_{Au} = 1.55$ J m^{-2} and $\gamma_{Re} = 3.13$ J m^{-2} [39].

To this end we did not discuss the interesting fact that the first superstructure that appears at all upon variation of coverage is the (1 × 3) phase. No low-coverage (1 × 1) phase nor a low-coverage (1 × 2) phase could be observed, despite a careful search including a variation of the preparation parameters (deposition rate, sample temperature, annealing). Viewing at our structure model(s) of figure 9 we state that the (expected) adsorbate structure, in which every Re trough carries a gold chain (hypothetical coverage = 1.0) does simply not appear, and similarly, we must emphasize the lack of another (not unlikely) structural feature, in which a local 'triple' chain of Au atoms represents a structural motif. It would lead to a (1 × 2) LEED pattern and be associated with a coverage of $\Theta_{1\times2} = 1.0$. The reason(s) why these structures are not formed are beyond our present knowledge of the system's properties and represent kind of a challenge for (hopefully) upcoming quantum-chemical or statistical-mechanical calculations.

Our LEED structure analysis of the Au(1×1) phase (which includes a quantitative Au coverage determination) enables us to expand somewhat on the bonding geometry of Au on Re, i.e., on the Au–Au and Au–Re bond lengths at the Au–Re interface. The LEED I, V analysis yielded a surface relaxation of +3% and +6% for the first two adsorbed Au layers, respectively, as compared to the ideally terminated Re hcp crystal. The respective layer distances of 0.82 and 1.69 Å render a determination of the Au–Au and Au–Re bond length possible. The Au–Re bond length for the Au atoms adsorbed next to the Re rows are 2.86 (±0.02) Å, while the Au–Re distance for the Au atoms located in the Re troughs comes out to 2.84 (±0.02) Å. The Au–Au bond length between the Au atoms located in the troughs and on the rows is 2.75 (±0.02) Å. We recall that the bond distance between two adjacent Au atoms in [1$\bar{2}$10] direction is only 2.761 Å, i.e., identical to the Re lattice constant a_{Re}. Compared to bulk gold the Au–Au distances are markedly compressed in both directions. This provides us with a straightforward explanation for the appearance of the (1 × n) phases: apparently, the elastic forces due to the Au compression can be somewhat released by a slight shift of the Au atoms in the direction of the unoccupied rows and a modulation of the vertical bond distances resulting in a moderate layer buckling. This is why we expect relaxations for all pseudomorphic structures within the (1 × n) phases ($n > 1$).

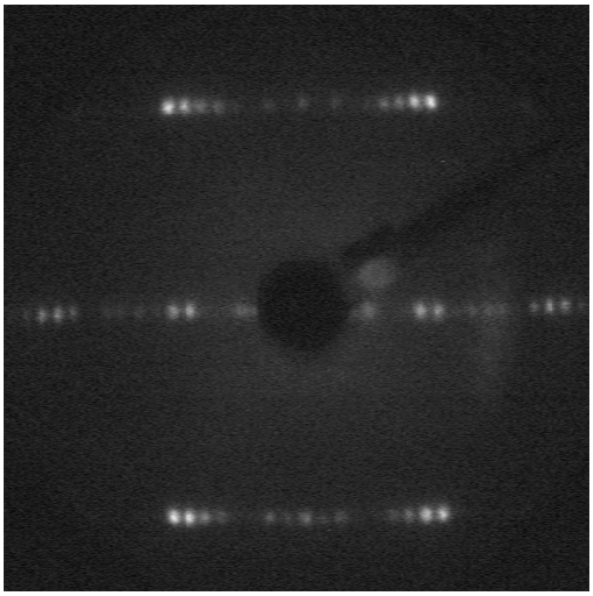

Figure 10. Reproduction of the LEED pattern of the reconstructed Au(1 × 8) phase, electron energy 26 eV. The (0, 0) spot is shadowed by the Re crystal.

3.4. Ordered Au phases in the multilayer regime

Next we turn to Au coverages $\Theta > 2$ (= multilayer concentrations in our coverage definition). When we continue to deposit Au at 800 K, the (1 × 1) LEED phase changes in that new 'extra' spots of a (1 × 8) structure appear as reproduced in the LEED pattern of figure 10. Quite interestingly, this (1 × 8) phase persists, almost independent of the Au coverage, at least up to $\Theta = 4$ (4 bilayers = 8 ML). We note that in parallel MEED experiments there is no further rise in intensity beyond the second maximum at $\Theta = 2$, rather, the MEED intensity decreases continuously, cf, figure 4. This behavior allows valuable conclusions on the type of growth for $\Theta > 2$ in that it rules out a strict layer-by-layer growth which would lead to periodic MEED oscillations. Instead, the mesoscopic roughness seems to increase steadily. On the other hand, our LEED observations do not support the occurrence of a strict three-dimensional growth, since we do not find running or split spots which would indicate faceting (growth of pyramids) or a gradual reconstructive transition to the genuine bulk gold structure. In view of surface free energy properties of Au and Re, three-dimensional (cluster) growth is also quite unlikely, especially at the elevated temperatures of our deposition experiments. From the development of the intensity of the (1 × 8) fractional-order beams, $I_{1\times8}$, we can, nevertheless, deduce some information on the growth mechanism. Initially, $I_{1\times8}$ increases steeply with Au coverage until beyond $\Theta = 1.5$–1.75 (bilayers or 3–3.5 ML) the respective increase falls somewhat but continues until $\Theta = 4$, the highest coverage studied in our work. The fact that this (1 × 8) intensity increase still persists up to fairly large coverages can only be reconciled with the assumption that not the entire 4-bilayer Au film is (1 × 8) oriented, but rather a (1 × 8)-oriented surface layer kind of floats on top of the bulk

Au film (which is still pseudomorphic with respect to the Re surface, see below). In essence, the Au growth mechanism in the multilayer regime can be described as an (incomplete) pseudomorphic layer-by-layer type growth with more or less flat terraces but with a (1 × 8)-reconstructed layer on top. We note that in previous work on the Au/Re(10$\bar{1}$0) system performed in our own laboratory [40] even coverages as high as 10 bilayers were studied, and still the (1 × 8) phase persisted up to these coverages.

We may therefore conclude that up to Au coverages of more than 4 bilayers a gold crystal with its inherent bulk structure is not stable, rather, a stack of Au layers pseudomorphic to the Re(10$\bar{1}$0) surface orientation, with a (1 × 8) reconstructed top layer is formed. In other words, we may have succeeded in preparing *a couple of layers of hcp-oriented gold*, similar to (apparently successful) attempts to grow fcc cobalt epitaxially on top of fcc-oriented Ag or Cu(100) surfaces [25, 41]. Further evidence could be obtained from surface x-ray diffraction or photoelectron diffraction experiments.

Concerning the structure of the (1 × 8) reconstructed phase we propose a coincidence structure with a uniaxially distorted (compressed) close-packed layer. Uniaxial compressions seem to be typical for hexagonal gold surfaces and have been reported to occur in the [1$\bar{1}$0] direction of the Au(111) surface to explain its unique ($\sqrt{3}$ × 22) rect surface reconstruction [42, 43]. To model our (1 × 8) reconstructed surface phase various domains having different registry with respect to the substrate are conceivable; two possibilities are indicated in the ball models of figure 11 (top view and side view). In possibility #1 the first Au atom in [1$\bar{2}$10] direction is located in a bridge site, whilst in possibility #2, the respective Au atom resides in a 4-fold coordinated site provided by the pseudomorphic (1 × 1) Au bilayer. The vertical positions drawn in figure 11 arise from considering the hard sphere radii of the Au and the Re atoms, respectively. In reality, the 'floating' top layer (and, likely, also the layer(s) underneath) will certainly relax to minimize the surface free energy. We have chosen possibilities #1 and #2, because they represent the structures with the highest symmetry. Both possess a mirror plane parallel to the [0001] and to the [1$\bar{2}$10] direction, respectively. Concerning the 'imaging' of such a structure in a LEED experiment, it is certainly not possible to distinguish a 'true' (1 × 8) phase from a mere coincidence structure, since multiple scattering effects and buckling phenomena will generate both the correct adsorbate and substrate spots and the appropriate modulation of the scattering potential. Within our coincidence model we interpret the observed (1 × 8) LEED pattern in a way as it is sketched schematically in figure 12. Shown are both the (1 × 8) and the (1 × 1) reciprocal unit cells, whereby the larger open circles represent the Re (10$\bar{1}$0) substrate beams (0, 0; 0, 1; −1, 1; 0, −1) and the large shaded circles indicate the lattice points of the uniaxially compressed reciprocal hexagonal mesh. The small open circles arise from the coincidence of both lattices. If the Au film grows in several layers in this configuration, we would expect all spots marked by open circles to gradually disappear and the hexagonal structure to take over and dominate the LEED pattern. This is, however, not the case.

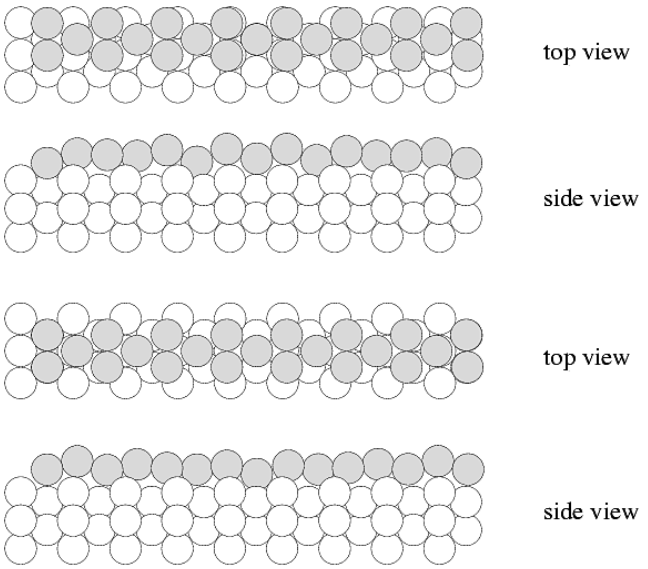

Figure 11. Ball models (top view and side view) for two kinds of coincidence structures possibly formed by Au atoms that squeeze into appropriate sites of the Re(10$\bar{1}$0) surface. See the text for further details. Again, Au atoms are drawn gray, Re atoms white.

In summary, we may compare the features of the reconstructed (1 × 8) phase with the likewise reconstructing Au(100) and Au(111) surfaces. A key feature for understanding the tendencies for the compressive reconstructions could be the fact that the Au–Au bond length in Au gas phase dimers is shorter (2.47 Å [44]) than the Au–Au distances in the bulk fcc crystal (2.885 Å), in other words, due to the reduced coordination in the surface the top Au atoms tend to come closer together in order to reduce somewhat the tensile stress. On Au(100) [42, 45] the dominating (1 × 5) LEED motif arises from of a coincidence between a uniaxially, 4% compressed hexagonally close-packed surface layer and the underlying (100) layer(s) of the bulk crystal. The aforementioned reconstruction of the Au(111) surface can be explained by a stacking of hcp and fcc like domains [43], and, similar to the (100) surface, involves a uniaxial compression of about 4%. In effect, this leads to a slight increase of the (local) Au surface atom density from 1.39 × 10^{19} atom m^{-2} to 1.445 × 10^{19} atom m^{-2}. Note that for our two (1 × 8) reconstruction models shown in figure 11 we end up with an Au surface atom density of 1.43 × 10^{19} atom m^{-2}; in terms of our coverage definition equal to $\Theta = 0.88$ (bilayers) or 1.76 Au monolayers, in excellent agreement with the density reported for the reconstructed Au(111) surface.

Following Ibach [46], the criterion for the appearance of pseudomorphism is a minimum misfit between the hypothetical (reconstructed!) Au surface lattice and the substrate surface lattice (in our case, the Re(10$\bar{1}$0) lattice), while the bulk lattice geometry is less decisive. In this respect it appears plausible that a pseudomorphic Au film on a surface of a foreign metal can very well exhibit less tensile stress than an Au surface on top of an Au substrate.

In view of this background we may return to the interesting fact that Poulston *et al* [34] explicitly reported

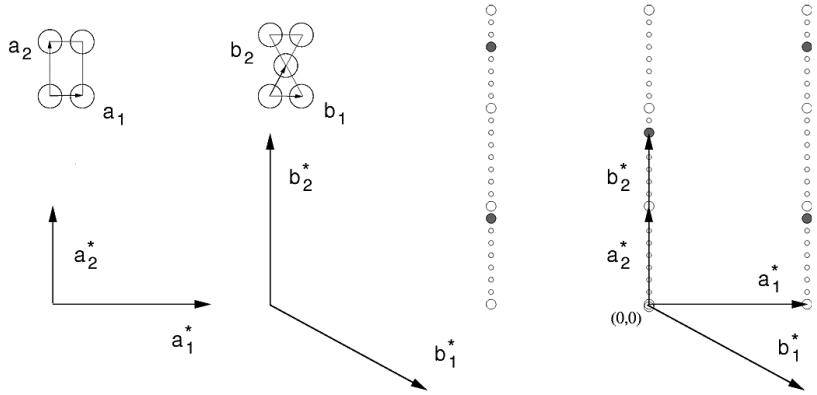

Figure 12. Interpretation of the (1 × 8) LEED pattern as being caused by a superposition of both a quasi-hexagonal (1 × 8) unit mesh and the (1 × 1) unit mesh of the pseudomorphic Au layer(s) underneath. Indicated are the reciprocal lattice vectors $\vec{a}_1^*$ and $\vec{a}_2^*$ of the rectangular (1 × 1) mesh and b_1^* and b_2^* of the quasi-hexagonal surface unit cell. The larger open circles represent the Re $(10\bar{1}0)$ substrate beams while the large shaded circles the lattice points of the uniaxially compressed hexagonal mesh. The small open circles arise from the coincidence of both lattices.

the lack of pseudomorphic growth of Au on the ruthenium $(10\bar{1}0)$ surface. The most prominent difference with respect to our Re$(10\bar{1}0)$ surface is undoubtedly the smaller Ru lattice parameter of 2.695 Å and, hence, the smaller unit mesh, and it is easily feasible that the tensile stress (even of reconstructed) Au films is too large for the Au atoms to accommodate on the Ru lattice and to form a pseudomorphic layer. This does probably not affect the formation of the (1 × *n*) phases, since here a lateral relaxation of the Au chains in [0001] direction can relieve the strain and is still possible as long as 'empty' Ru rows interrupt the Au chains.

Another point raised by Poulston *et al* is the growth mechanism of Au in the multilayer regime; for their Ru$(10\bar{1}0)$ surface they claim from XPS and Auger data that simultaneous multilayer ('SM') growth occurs rather than pseudomorphic layer-by-layer growth. In addition, they do not find a (1 × 8) reconstructed Au phase as the multilayers form on top of the (1 × *n*) phases, instead they need deposition of more than 15 Au monolayers to obtain indications of a new LEED pattern from which they deduce a structural rearrangement of their Au film towards a compact Au(111) crystal [34].

In conclusion, we have shown that gold grows pseudomorphically on a Re$(10\bar{1}0)$ surface, after it has formed several ordered (1 × *n*) phases in the submonolayer range which consist of Au chains along $[1\bar{2}10]$ direction which continuously coalesce. For the Au(1 × 1) phase we have performed a LEED *I*, *V* analysis and could conclude also from CO thermal desorption data that it consists of a full, somewhat relaxed, bilayer which could then be used to monitor the absolute Au coverages of the sub-bilayer structures. We could also demonstrate that up to coverages of ∼8 bilayers the pseudomorphic, hcp-oriented Au film is covered by a uniaxially compressed Au monolayer that gives rise to a (1 × 8) coincidence LEED pattern.

Acknowledgments

We gratefully acknowledge financial support by the Deutsche Forschungsgemeinschaft through SPP 1091 and technical help by R Cames and K Schubert.

References

[1] Bauer E 1982 *Appl. Surf. Sci.* **11/12** 479
[2] Bauer E 1991 *Ber. Bunsenges. Phys. Chem.* **95** 1315 and references therein
[3] Bauer E 1984 *The Chemical Physics of Solid Surfaces and Heterogeneous Catalysis* vol 3, ed D A King and D P Woodruff (Amsterdam: Elsevier) chapter 1
[4] Wissmann P (ed) 1987 Thin metal films and gas chemisorption *Studies in Surface Science and Catalysis* vol 32 (Amsterdam: Elsevier)
[5] Campbell C T 1990 *Annu. Rev. Phys. Chem.* **41** 775
[6] Brune H 1998 *Surf. Sci. Rep.* **31** 121
[7] Binnig R, Rohrer H, Gerber C and Weibel E 1982 *Phys. Rev. Lett.* **49** 57
[8] van Hove M A, Moritz W, Over H, Rous J P, Wander A, Barbieri A, Materer N, Starke U and Somorjai G A 1993 *Surf. Sci. Rep.* **19** 191
[9] van Hove M A and Tong S Y 1979 *Surface Crystallography by LEED* (Berlin: Springer)
[10] Rous P J, Pendry J B, Saldin D K, Heinz K, Müller K and Bickel N 1986 *Phys. Rev. Lett.* **57** 2951
[11] Parschau M, Schlatterbeck D and Christmann K 1997 *Surf. Sci.* **376** 133
[12] Wagner R, Schlatterbeck D and Christmann K 1999 *Surf. Sci.* **440** 231
[13] Payne S H, LeDue J M, Michael J C, Kreuzer H J, Wagner R and Christmann K 2002 *Surf. Sci.* **512** 151
[14] Wagner R 2002 *PhD Thesis* Free University Berlin
[15] Pauls C, Przyrembel D and Christmann K 2004 *J. Phys. Chem.* B **108** 14749
[16] Pauls C and Christmann K 2005 *Presented at the (ECOSS 23): 23rd Int. Conf. Surf. Sci. (Berlin)* in preparation
[17] Lenz J, Rech P, Christmann K, Neuber M, Zubrägel C and Schwarz E 1992 *Surf. Sci.* **269/270** 410
[18] Wagner R and Christmann K 2009 in preparation
[19] Heinz K and Hammer L 1997 *Phys. Status Solidi* a **159** 225
[20] Davis L E 1994 *A Reference Guide to the IRAF/DAOPHOT Package* National Optical Astronomy Observations http://iraf.noao.edu
[21] Pendry J B 1974 *Low-Energy Electron Diffraction* (London: Academic)
[22] Davis H L and Zehner D M 1980 *J. Vac. Sci. Technol.* **17** 190
[23] Döll R, Hammer L, Heinz K, Bedürftig K, Muschiol U, Christmann K, Seitsonen A P, Bludau H and Over H 1998 *J. Chem. Phys.* **108** 8671

[24] Pauls C *PhD Thesis* FU Berlin in preparation
[25] de Miguel J J, Cebollada A, Gallego J M, Ferrer S, Miranda R, Schneider C M, Bressler P, Garbe J, Bethke K and Kirschner J 1989 *Surf. Sci.* **211/212** 732
[26] Blum V, Hammer L, Meier W and Heinz K 2001 *Surf. Sci.* **488** 219
[27] Sporn M, Platzgrummer E, Forsthuber S, Schmid M, Hofer W and Varga P 1998 *Surf. Sci.* **416** 423
[28] Kottcke M and Heinz K 1997 *Surf. Sci.* **376** 352
[29] Blum V and Heinz K 2001 *Comput. Phys. Commun.* **134** 219
[30] Heinz K 1995 *Rep. Prog. Phys.* **58** 637
[31] Pendry J B 1980 *J. Phys. C: Solid State Phys.* **13** 937
[32] Houston J E and Park R L 1970 *Surf. Sci.* **21** 209
[33] Ertl G and Küppers J 1985 *Low-Energy Electrons and Surface Chemistry* (New York: VCH/Weinheim)
[34] Poulston S, Tikhov M and Lambert R M 1995 *Surf. Sci.* **331–333** 818
[35] Gottfried J M, Schmidt K J, Schroeder S L M and Christmann K 2003 *Surf. Sci.* **536** 206
[36] Ertl G and Rau P 1969 *Surf. Sci.* **15** 443
[37] Harendt C, Christmann K, Hirschwald W and Vickerman J C 1986 *Surf. Sci.* **165** 413
[38] Schröder J, Günther C, Hwang R Q and Behm R J 1992 *Ultramicroscopy* **42–44** 475
[39] Tyson W R and Miller W A 1977 *Surf. Sci.* **62** 267
[40] Vollmer A 1999 Wachstum und Struktur von dünnen Silber- und Goldfilmen auf einer Rhenium($10\bar{1}0$)-Oberfläche *PhD Thesis* Free University Berlin
[41] Schneider C M, Bressler P, Schuster P and Kirschner J 1990 *Phys. Rev. Lett.* **64** 1059
[42] van Hove M A, Koestner R J, Stair P C, Biberian J P, Kesmodel L L, Bartos I and Somorjai G A 1981 *Surf. Sci.* **103** 189
[43] Barth J V, Brune H, Ertl G and Behm R J 1990 *Phys. Rev.* B **42** 9307
[44] Feibelman P J 1997 *Phys. Rev.* B **56** 2175 reference [48]
[45] Palmberg P W and Rhodin T N 1967 *Phys. Rev.* **161** 586
[46] Ibach H 1997 *Surf. Sci. Rep.* **29** 193